Journal of Power Sources 233 (2013) 331–340

Contents lists available at SciVerse ScienceDirect

Journal of Power Sources

journal homepage: www.elsevier.com/locate/jpowsour

Ni/YSZ solid oxide fuel cell anodes operating on humidified ethanol fuel feeds: An optical study

Michael B. Pomfret [a,*], Daniel A. Steinhurst [b], Jeffrey C. Owrutsky [a]

[a] U.S. Naval Research Laboratory, 4555 Overlook Avenue, Washington, DC 20375, USA
[b] Nova Research, Inc., 1900 Elkin Street, Suite 230, Alexandria, VA 22308, USA

HIGHLIGHTS

- Direct steam reforming of C_2H_5OH in SOFCs investigated by NIR thermal imaging.
- Humidified fuel flows result in far less damage to the anode than dry ethanol.
- Imaging and spectroscopy characterize reforming in the gas phase and at the anode.
- Limiting carbon formation with <3:1 H_2O:C_2H_5OH is promising regarding logistics.
- Real-time analysis of SOFC failure demonstrates diagnostic capabilities of imaging.

ARTICLE INFO

Article history:
Received 9 August 2012
Received in revised form
8 January 2013
Accepted 10 January 2013
Available online 21 January 2013

Keywords:
Solid oxide fuel cell
Ethanol
Thermal imaging
Steam reforming
Infrared

ABSTRACT

Direct internal steam reforming of ethanol fuel in solid oxide fuel cells (SOFCs) has been investigated using near-infrared thermal imaging. Thermal data are correlated to electrochemical analyses, post-mortem photographs of the cells and gas-phase infrared (FTIR) spectroscopy. These techniques allow for an understanding of how gas-phase composition and electrical conditions affect the fuel chemistry on the anode, specifically with regards to carbon formation. Ethanol flows that are humidified to H_2O:C_2H_5OH ratios of 1.58, 1.27, and 1.12 at 700, 750, and 800 °C, respectively, result in far less anode damage than dry ethanol. However, subtle spatial variations in anode surface temperature indicate that damage occurs at temperatures below 800 °C. FTIR spectra of the fuel feed reaching the anode show that internal steam reforming occurs both in the gas phase and at the anode catalyst. Thermal imaging and post-mortem analysis confirm that humidified ethanol flows at 800 °C form negligible amounts of carbon deposits in polarized cells, resulting in minimal anode deterioration. These results serve as benchmark data for the further development of direct, internal reforming SOFC systems, especially in smaller, portable systems. The H_2O:C_2H_5OH ratio used in this work is well below the >3:1 ratios suggested elsewhere.

1. Introduction

Many types of fuel cells, including solid oxide fuel cells (SOFCs), are being investigated as future alternative power sources for a variety of stationary and portable applications. [1] Compared to other types of fuel cells, a clear benefit of SOFCs is their tolerance for carbon-based fuels due to the high operating temperatures (>600 °C) needed for oxide conduction through the electrolyte. [2,3] At these temperatures, activation barriers to fuel oxidation and oxygen reduction are not rate-limiting, and carbon monoxide (CO) and carbon dioxide (CO_2) are not irreversibly adsorbed to catalyst surfaces. These properties have positioned SOFCs as attractive power sources for renewable fuels and as a bridge from the current petroleum-dominated infrastructure to an alternative fuel economy. The performance of many types of hydrocarbon fuels has been tested for SOFCs with varying degrees of success [1,4–8]. Generally, the standard Ni/yttria-stabilized zirconia (YSZ) cermet anode material has proven to be susceptible to degradation due to coking from hydrocarbons [8–21]. Many solutions have been proposed to curb – or eliminate – deleterious processes at the anode. One approach is to use other anode materials that are less susceptible to degradation by hydrocarbons [22–30]. Ceria-based catalysts can operate cleanly with a variety of fuels, ranging from methane to heavier hydrocarbons – *i.e.*, butane – to alcohols

* Corresponding author. Tel.: +1 202 404 2554; fax: +1 202 404 8119.
E-mail addresses: michael.pomfret@nrl.navy.mil (M.B. Pomfret), daniel.steinhurst.ctr@nrl.navy.mil (D.A. Steinhurst), jeff.owrutsky@nrl.navy.mil (J.C. Owrutsky).

0378-7753/$ – see front matter © 2013 Elsevier B.V. All rights reserved.
http://dx.doi.org/10.1016/j.jpowsour.2013.01.048

[23,27,29,31]. However, ceria anodes are less catalytically active than Ni/YSZ cermets. Another way to reduce carbon formation while maintaining the highest electrical output possible is to use fuel additives to partially oxidize hydrocarbons which reduces their propensity to form deposits on Ni/YSZ anodes [8,11,13,32–35]. This is often accomplished through external or internal steam reforming of the fuel, which increases the complexity of the system and adds the requirement of a clean source of water to the SOFC assembly.

A third option for the clean operation of Ni/YSZ anodes is to use alcohol-based fuel feeds that intrinsically include oxygen in the fuel [17,32,36,37]. In the thermodynamic limit, coking is reduced by a fuel stream with a low carbon-to-steam or carbon-to-oxygen (C:O) ratio. Methanol (CH_3OH) and ethanol (C_2H_5OH) are relatively abundant renewable fuels that can be produced from a variety of sources, including petroleum and renewable biomass. Both fuels have low carbon-to-oxygen ratios within the fuel molecule. This promotes cleaner cell operation through partial oxidation processes, such as gas-phase pyrolysis. In CH_3OH the C:O ratio is 1:1, making it more likely that CH_3OH can be used cleanly under typical SOFC operating conditions. However, previous spectroscopic and imaging studies have shown CH_3OH to coke anodes at temperatures below 800 °C [17,38]. Conventional experimental and theoretical studies also show that CH_3OH will form carbon deposits under a number of conditions [36,39,40].

C_2H_5OH has a 2:1 C:O ratio, so not all of the C atoms in the fuel will be oxidized to CO through pyrolysis. Previous experimental and computational studies of SOFCs with C_2H_5OH fuel have shown promise for long operation free of carbon deposits contingent upon the conditions and whether gas-phase pyrolysis reaches equilibrium [10,11,19,23,32,41]. The factors contributing to C_2H_5OH performance and degradation are important to recognize and understand in order to achieve efficient and durable operation. Both Cimenti and Hill [11] and Sasaki et al. [32] have predicted that if C_2H_5OH fuel feeds are allowed to reach thermodynamic equilibrium at high enough temperatures (>800 °C), SOFCs can be operated without carbon-related performance losses. However, experiments by both groups indicate that C_2H_5OH flows do not reach equilibrium under realistic operating conditions [10,11,19,23,32]. These results are supported by kinetic models of C_2H_5OH pyrolysis published by Gupta et al., [41] which identify olefins and C_{5+} species in SOFC fuel streams and recognize them to be precursors to the species that ultimately form carbon deposits. Numerous experimental studies agree with the results of Cimenti and Hill, [11] Sasaki et al. [32] and Gupta et al. [41]. While a goal of using alcohol fuels is to avoid the use of partial oxidation processes for cleaner fuel feeds, steam reforming may be more logistically viable for C_2H_5OH operation if the amount of H_2O needed to prevent anode poisoning can be substantially reduced. Many published studies conclude that a molar H_2O:C_2H_5OH ratio of 3:1 or greater at temperatures of 800+ °C is needed to mitigate anode damage [8,31,42,43]. Such large amounts of H_2O relative to C_2H_5OH introduce logistical issues of providing the SOFC with a continuous supply of clean water. Work published by Cimenti and Hill suggest that H_2O:C_2H_5OH ratios <2:1 may be suitable for clean operation over a wide range of operational temperatures [11]. Recycling anode exhaust containing H_2O may further reduce the amount of steam needed [44].

Carbon deposition on Ni/YSZ – and the subsequent failure of the membrane electrode assembly (MEA) – presents a complicated problem to prolonged SOFC operation. Many traditional SOFC experiments rely on electrical characterization of MEAs that represent convolutions of the chemical and transport processes contributing to electrochemical performance. While voltammetry and impedance data produce useful results that are pertinent to how well the cell is operating, they typically are unable to identify chemical or material processes that underlie the observed behavior. Optical methods offer the ability to directly characterize cell chemistry *in situ* [45,46]. Initial *in situ* optical studies have included infrared (IR) emission and Raman spectroscopy [47,48]. Thermal imaging has also been demonstrated as useful for studying reactions occurring at SOFC electrodes by characterizing changes in anode surface temperatures (ΔT) [17,49–52].

This paper presents the results of near-IR (NIR) thermal imaging and spectroscopic studies for SOFCs supported by Ni/YSZ anodes operated with both dry and wet C_2H_5OH (DE and WE, respectively). In addition to thermal imaging studies of the anode temperature for WE fuels at various temperatures and cell potentials, the fuel composition was characterized with FTIR spectroscopy. A range of temperatures (700–800 °C) and cell voltages were used to understand how the operating conditions influence partial oxidation reactions in the gas-phase and anode surface processes. Results demonstrate that while humidification reduces anode susceptibility to failure compared to DE, the extent of internal reforming depends strongly on temperature. Observed changes in anode surface temperature (ΔT) indicate that internal steam reforming is insufficient for durable performance below 800 °C. The ability to detect the early signs of cell failure and to characterize their diminished nature with steam reforming while SOFCs are operating demonstrates the benefit of real-time imaging as a potential process monitoring technique for high-temperature power systems.

2. Experimental

2.1. Fuel cell assembly

MEAs used in this study were button cell SOFCs obtained from Materials & Systems Research, Inc. (MSRI, Salt Lake City, UT). The 25 mm diameter, tape-cast MEAs were supported by a ~0.8 mm thick, large grain, Ni/YSZ composite anode. Other layers included a small grain, Ni/YSZ 12 μm thick anode interlayer; a 10 μm thick YSZ electrolyte; a 15 μm thick, strontium-doped lanthanum manganate (LSM)/YSZ cathode interlayer; and a 50 μm thick LSM cathode. The structure and electrochemistry of this type of MEA have been characterized previously [12,53,54].

Gold-mesh (Alfa Aesar, #40931) attached to the anode with gold ink (BASF #A1644) served as the current collector. A platinum-mesh (Aldrich #298093) was attached to the cathode using a small amount of gold ink, to ensure adhesion to the cathode, and a full coat of Pt ink (Heraeus #6082). MEAs were attached anode-side-out to a 25.4 mm OD alumina tube (Sentrotech) with zirconia paste (Aremco Products, Inc. #552). A 50.8 mm OD alumina tube surrounded the alumina-supported MEA and a 50.8 mm diameter, 3.175 mm thick sapphire window (Swiss Jewel Co. #W50.00) was attached to one end of the outer alumina tube to contain the reactant and product gases while providing optical access to the anode. The rear of the assembly was sealed with RTV silicone-based paste (Permatex, Ultra-Copper). The assembled SOFC manifold was placed inside a tube furnace (Thermo Scientific, Model # F21135) and heated to the operating temperatures of 700, 750, and 800 °C. A K-type thermocouple (Omega) was positioned on the outside of the larger alumina tube to provide a temperature reference. A schematic of the optically accessible SOFC assembly has been published previously [45] and is included in the Supplementary data.

2.2. Gas flows

All flows were regulated with mass flow controllers (Celerity FC-260V-4S). Constant flows of 150 sccm Ar and 85 sccm air were delivered to the anode and cathode, respectively. A flow of

100 sccm H_2 was added to the anode for standard operation. To study the effects of DE fuel, the anode-side Ar flow was routed through a glass bubbler containing the alcohol without the H_2 flow. The resultant flow was calculated to be 7.8% C_2H_5OH by volume at 20 °C. The fuel feed was humidified by directing a portion of the anode-side Ar flow through a glass bubbler containing water. The amount of H_2O added to the fuel feed depends on the temperature at which the cells are operated in accordance with recipes published by Cimenti and Hill [11]. At 800 °C, the fuel flow is 2.3% C_2H_5OH and 2.6% H_2O – for a 1.12 H_2O:C_2H_5OH ratio; the H_2O:C_2H_5OH ratios are 1.27 and 1.58 at 750 °C and 700 °C, respectively.

2.3. Electrochemical characterization

Cell polarization was maintained and electrochemical measurements were conducted with a potentiostat (Gamry Reference 3000 Potentiostat/Galvanostat/ZRA). Linear-sweep voltammetry (LSV) scans were conducted between OCV (typically 1.05 ± 0.05 V) and 0 V at a rate of 100 mV s^{-1}. Electrochemical impedance spectroscopic (EIS) measurements were made at frequencies between 100 kHz and 0.2 Hz, inclusive, at a V_{DC} of 100 mV and a V_{AC} of 50 mV.

2.4. Thermal imaging measurements

Thermal images were acquired at 5 Hz with a Si-charged-coupled device (CCD) camera (AVT, Stingray F033B ASG) with an 18–108-mm focal length macro zoom lens (Navitar Zoom 7000) using collection software written in-house in LabView v8.5. A 720 nm long-pass filter (Hoya R72) was used to block emitted and ambient reflected visible light. NIR intensities were analyzed and displayed in real time while simultaneously recording and storing the data for post-processing of specific regions of interest.

Cells were operated at OCV or polarized to a voltage (ΔV_{OC}) of 0.3 V and 0.6 V to study the effects of relatively moderate and heavy current flows. ΔV_{OC} is referenced to the OCV such that $V_{cell} = OCV - \Delta V_{OC}$, *i.e.*, a 0.3 V ΔV_{OC} corresponds to a 0.70 V–0.80 V V_{cell}. After at least 30 s at a given voltage, C_2H_5OH fuel was introduced and the H_2 flow was terminated while maintaining the set voltage. To oxidize carbon deposits that resulted from fuel flow, the cells were operated under an Ar-only anode-side flow at a current equivalent to 2/3 of the maximum current under H_2 conditions for that given cell.

Post-collection, the intensity of each image pixel was processed into a temperature using a linear calibration derived from thermocouple readings at the operational temperature and at 50 °C below that point. The resultant surface temperatures can then be averaged both spatially and temporally. The average surface temperature of a specific region of the anode can be tracked over time. The spatial and temperature resolutions are typically 0.1 mm and 0.1 °C, respectively. Data processing procedures have been previously described [50].

2.5. Gas-phase Fourier-transform infrared (FTIR) spectroscopy

FTIR spectra were taken of flows after transit through an alumina tube that was centered in the 40-cm long tube furnace in separate experiments. DE and WE fuel flows backed by 150 sccm Ar were fed through the furnace at temperatures of 700 °C, 750 °C, and 800 °C. The alumina tube had the same diameter (0.6 cm) as the fuel delivery tube in the SOFC assembly and the residence time at each operating temperature is estimated to be ~0.4 s, similar to the residence time of the fuel in the region of the SOFC assembly that is at operational temperature. The effluent was collected in a 10-cm pathlength, flow-through, gas-phase IR cell (New Era Enterprises, Inc. # 66005-10) with 6-mm thick zinc sulfide windows. 16-scan spectra were taken at a resolution of 2 cm^{-1} with a Matteson IR-7020 spectrometer.

3. Results

3.1. SOFC electrochemistry

The electrochemical performance of each cell is monitored by LSV and EIS periodically throughout the optical experiments. Electrochemical measurements are made under standard H_2 flows (defined above) before each exposure to alcohol to monitor cell function. Typical LSV and power density plots are shown in Fig. 1. The expected general trend of increased output with increased temperature is observed. The reported experiments are designed to allow for the study of the early stages of carbon/anode interaction at different voltages on the same cell to maximize efficiency and reduce the ambiguities of cell-to-cell variations. One way this is accomplished is by electrochemically oxidizing the anode after each exposure to C_2H_5OH flows. Typically, four cycles of C_2H_5OH exposure and anode oxidation are completed before the maximum current density falls below 75% of the initial value at which point the experiment is terminated. EIS data prior to each exposure to WE at 700 °C (Fig. 2) show the changes in resistances that occur with each cycle. Over the course of a WE experiment the bulk resistance typically increases 5–10%, compared to 20–30% after four cycles of a DE experiment.

3.2. FTIR analysis of reformed C_2H_5OH fuel feeds

Gas-phase FTIR spectroscopy has been used to identify the species present at the SOFC anode in our assembly as a result of DE fuel pyrolysis [17]. CO, CH_4, C_2H_4, and an unspecified C_6 molecule are all detected in the fuel flow. Unreacted C_2H_5OH is the most abundant fuel molecule to be identified by FTIR, comprising more than 90% of the total observed carbon species at 700 °C and more than 50% at 800 °C. In DE flows at all operational temperatures studied, CH_4 and C_2H_4 are the two most prominent pyrolysis products and both are known to form carbon deposits [11,23,41,55,56]. CO content is less than 2% of the observed carbon species. One reason for the excessive carbon deposition with DE flows is clear; pyrolysis is incomplete after ~0.4 s residence time at all operational temperatures, agreeing with previous work [41]. Furthermore, there is not a large presence of oxidized species that

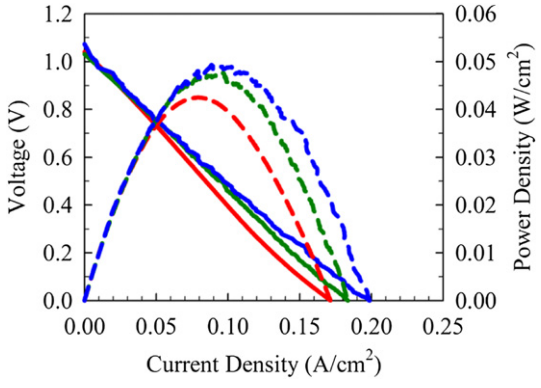

Fig. 1. Typical VI curves (—) and power density plots (–) of button cell SOFCs in the optical assembly operated at (red) 700 °C, (green) 750 °C, (blue) 800 °C. (For interpretation of the references to color in this figure legend, the reader is referred to the web version of this article.)

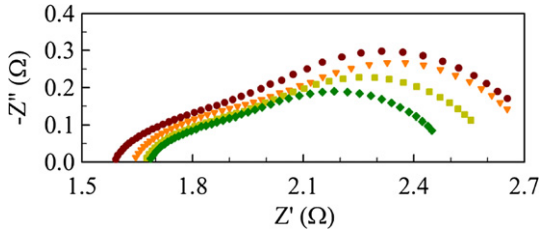

Fig. 2. Nyquist impedance plots typical of cells operated 700 °C (●) prior to exposure to wet ethanol, (▼) after one wet ethanol/oxidation cycle, (■) after two cycles, (◆) after three cycles.

participate in internal reforming reactions on the anode catalyst. Instead, both surviving C_2H_5OH and C_2H_5OH pyrolysis products form coke on the anode.

FTIR spectra of the WE flows are strikingly different than the DE flows at all three operational temperatures (Fig. 3). The carbon species that are detected in reformed WE flows and their respective concentrations in terms of the percent of observed carbon species are presented in Fig. 4. C_2H_5OH is still present, but at much lower concentrations. The unreacted fuel is not a majority species at any of the three temperatures studied and comprises only 3% of the observed carbon species at 800 °C. C_2H_5OH, CH_4, and C_2H_4 make up nearly 70% of the carbon content at 700 °C, which is greatly improved from DE flow at 700 °C but only ~10% less than the "best" DE condition at 800 °C. At 750 and 800 °C, temperatures at which carbon deposition is greatly reduced, CO becomes the dominant carbon species. However, C_2H_4 and CH_4 concentrations grow with increasing temperature, indicating that gas-phase steam reforming alone is not sufficient to partially oxidize C_2H_5OH to preclude anode coking.

3.3. NIR imaging of SOFC anodes with WE

False-color NIR images of the anodes of cells operated with WE for 10 min (Fig. 5) show smaller ΔT's than those observed with DE. The cooling that does occur is more intense in the central region of

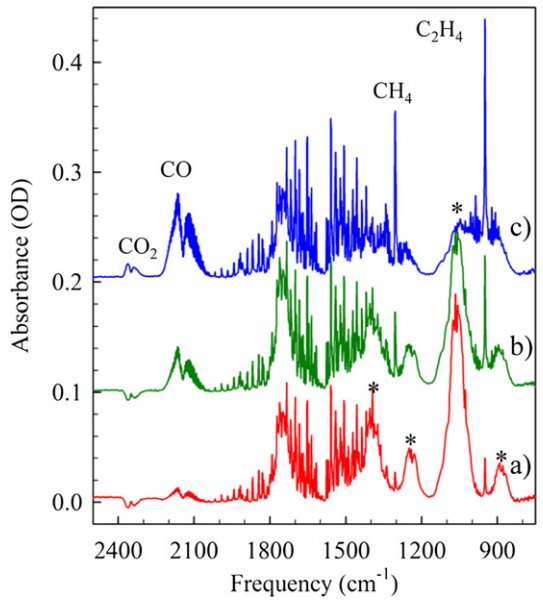

Fig. 3. FTIR spectra of wet ethanol flows with 0.4 s residence time at a furnace temperature of (a) 700 °C, (b) 750 °C, and (c) 800 °C. IR gas cell length is 10 cm. C_2H_5OH bands are indicated with an asterisk (*).

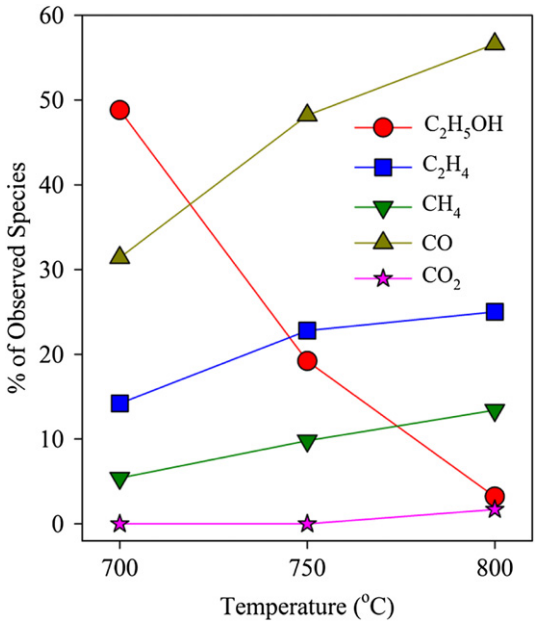

Fig. 4. Molar fraction of observed carbon species in wet ethanol fuel flows determined from observed vibrational bands in FTIR spectra for (●) C2H5OH, (■) C2H4, (▼) CH4, (▲) CO, and (★) CO_2.

the anode between the fuel inlet and the current collector – referred to as the region of interest (ROI); however, the spatial variation in surface temperature is muted compared to DE flows. The most dramatic difference between DE and WE flows is observed at 800 °C. The average ΔT of the ROI at OCV is -2.0 ± 0.2 °C under WE conditions, compared to ~−4.5 °C under DE conditions (Fig. 6). The plot of the average surface temperature in the ROI also reveals that polarizing the cell to 0.6 V ΔV_{OC} under WE results in a ΔT of −1.5 °C. Under DE, the cell cools by approximately the same amount whether polarized or at OCV. Cells operated at 700 and 750 °C cooled less than cells under DE. However, the typical trend of less surface cooling with increasing ΔV_{OC} due to anode oxidative heating is not observed (Fig. 7). For polarized SOFCs, ΔT is lower, but cells generally cool more when ΔV_{OC} is 0.6 V than at 0.3 V despite a higher expected current density at the former voltage. This serves as an indication of carbon deposition, *vide infra*.

The spatial variations in Fig. 5 can be demonstrated by plotting the ΔT for each pixel across a horizontal profile centered in the ROI (Fig. 8). The profiles shown are representative data from one cell for each set of conditions and exhibit the same trends as other cells operated at the respective conditions. The profile lines are drawn approximately halfway between the fuel inlet and the current collector. The profile lengths vary depending on slight differences in the manual placement of the lines. The temperature variation across the anodes of cells at OCV exposed to DE at all three operational temperatures show maximum ΔT's of 4–7 °C with the most intense cooling occurring near the center of the profiles in the path of the fuel flow. WE flows result in varied temporal and spatial ΔT profiles that depend greatly on the operational temperatures. At 700 °C the portion of the profile in the flow path cools ~3 °C. The outer regions of the profile only cool ~1 °C, resulting in a relatively sharp, spatially-defined area of cooling that is likely due to carbon deposition. The sharper regional ΔT's are not evident at 750 °C. The anode surface still cools more in the middle of the profile, but only ~1 °C more than the outer regions. At 800 °C the ΔT's are most subtle of the operational temperatures studied. The maximum ΔT, again in the center of the profile, is less than −2 °C.

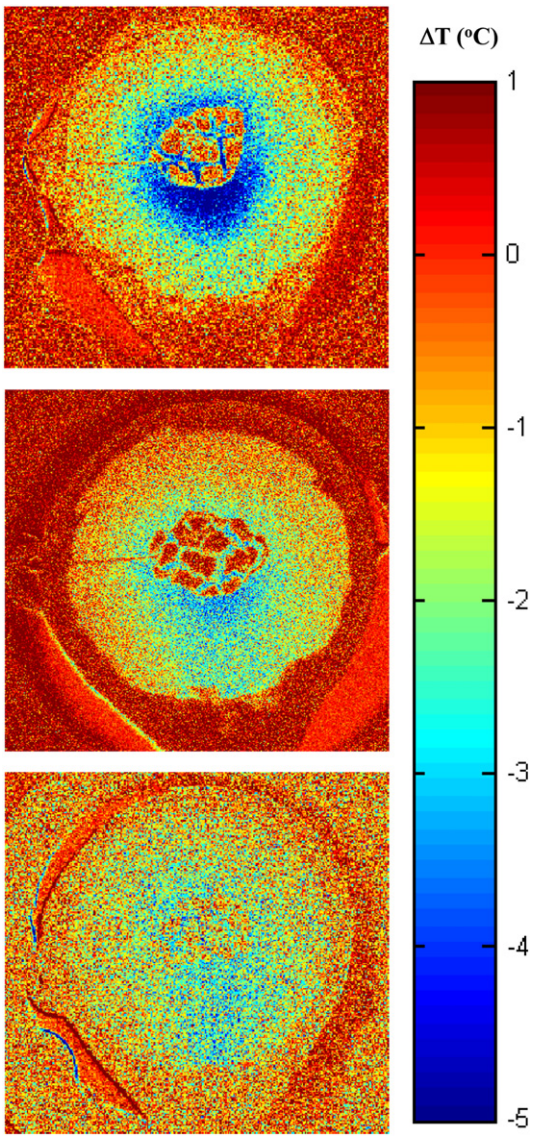

Fig. 5. False-color thermal images showing the change in surface temperature of SOFC anodes under OCV conditions exposed to 10 min of wet ethanol at (top) 700 °C, (middle) 750 °C, and (bottom) 800 °C.

The degree of cooling is an indication of more abundant or faster fuel cracking reactions that may result in more carbon formation. A more reliable method for qualitatively determining the amount of carbon on the surface after exposure to fuel flows is to track ΔT while anodes – and any carbon on them – are electrochemically oxidized by heavily polarizing the MEAs while only flowing Ar in the anode chamber.

Temporal profiles of the electrochemical oxidation of anodes following exposure to WE are shown in Fig. 9. At 700 °C, ΔT is ~+2 °C at the onset of electrochemical oxidation, which is much smaller than the ~+4 °C ΔT that is observed with DE [17]. This amount of heating is sustained for 4–5 min before the anode surface begins to cool. After 10 min, the temperature has not decreased to its initial level, serving as evidence that the oxidation process is prolonged as would be expected when carbon is deposited throughout the anode structure. At 750 and 800 °C the heating profiles are similar to those observed in cells not exposed to carbon. The 750 °C trace peaks between 1.0 and 1.5 °C at ~2 min, before immediately beginning to cool. The anode operated at 800 °C heats

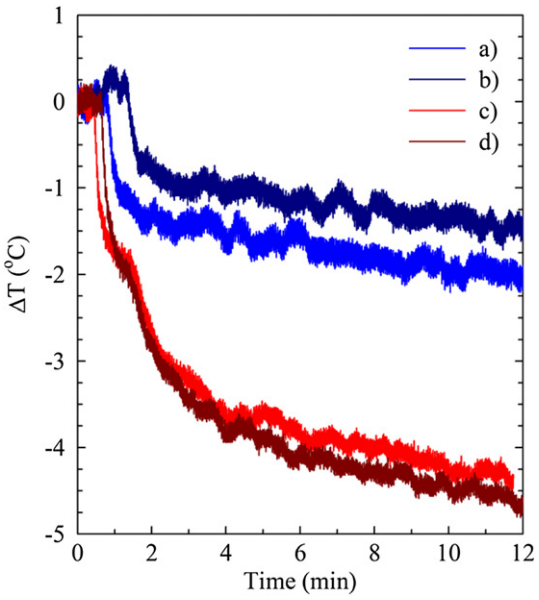

Fig. 6. The spatially-averaged ROI ΔT of anodes exposed to (a) wet ethanol at OCV, (b) wet ethanol at 0.6 V ΔV_{OC}, (c) dry ethanol at OCV, and (d) dry ethanol at 0.6 V ΔV_{OC} during a 10 min fuel exposure at 800 °C.

only 0.5 °C. In both cases, ΔT drops below 0 °C suggesting complete oxidation.

Given the success of steam reforming using the 1.12 H_2O:C_2H_5OH ratio at 800 °C and the logistical concerns of a constant source of H_2O, an attempt was made to characterize the results with less water by reducing the relative amount of H_2O by a factor of two in the fuel stream. ΔT's on anodes exposed to feeds with a 0.56 H_2O:C_2H_5OH ratio are similar to those observed for anodes exposed to DE feeds.

3.4. Comparing in situ data to post-mortem results

Pictures of MEAs operated with both DE and WE taken after operation and cool-down under Ar clearly show the difference in anode degradation when steam reforming occurs (Fig. 10). Prior to

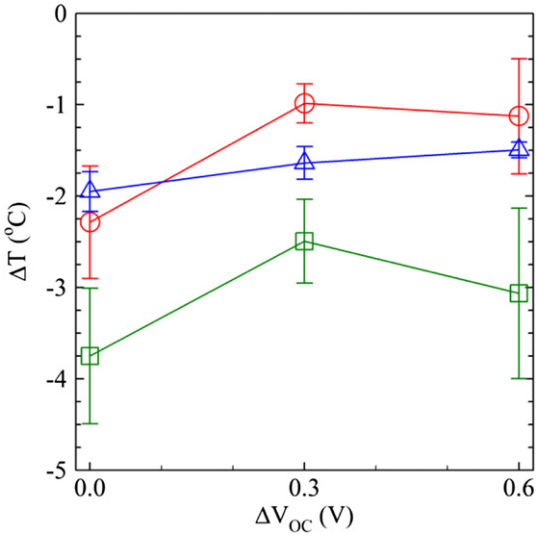

Fig. 7. Voltage dependence of multiple-cell averages of the spatially-averaged ROI ΔT that results from wet ethanol exposure at (○) 700 °C, (□) 750 °C, and (△) 800 °C.

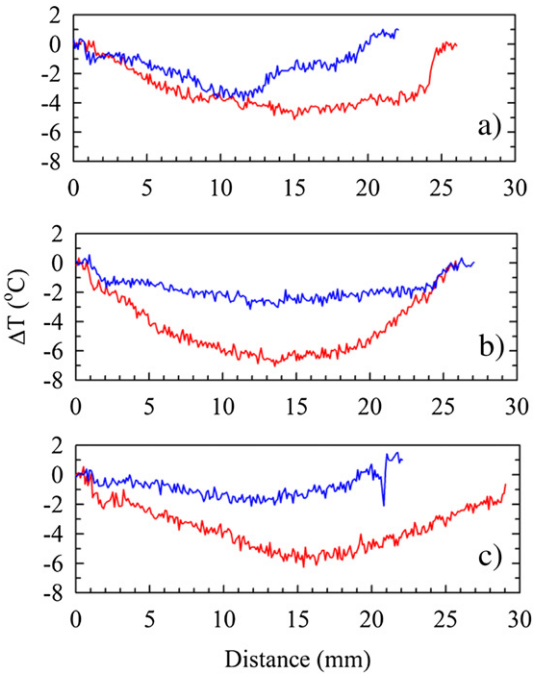

Fig. 8. Horizontal spatial profiles of anode Δ*T* during exposure to (red) dry ethanol and (blue) wet ethanol at (a) 700 °C, (b) 750 °C, and (c) 800 °C. (For interpretation of the references to color in this figure legend, the reader is referred to the web version of this article.)

cool-down and disassembly the cells are operated under electrochemically oxidizing conditions so all anodes appear dark green–gray. Cells operated with DE at all temperatures show extensive damage, which appears as discoloration to lighter shades of green–gray (outlined in red in Fig. 10). The light color of the anodes is most likely due to Ni removal from the anode structure resulting from metal dusting, a process known to accompany carbon deposition in SOFCs [57]. Damage is greatly reduced when WE is used, which is indicative of less carbon deposition. However, cells still show discoloration, especially directly in front of the fuel inlet, which has been shown to be symptomatic of anode fatigue [17]. The cell operated at 700 °C (Fig. 10a) exhibits minor-to-moderate discoloration that extends past the current collector to cover most of the anode surface. Damage to the cell operated at 750 °C is less extensive. Typically, the discoloration in cells operated at this temperature spreads approximately half-way across the anode surface. The shape of the discolored region in Fig. 10c is an indication of a flow path that is slightly off-axis with the center of the cell. At 800 °C (Fig. 10e), the discolored region is reduced to a small area directly adjacent to the fuel inlet. The cracking of the cell occurred during the cooling and dismantling of the SOFC assembly and is not an indication of damage incurred while the cell was functioning.

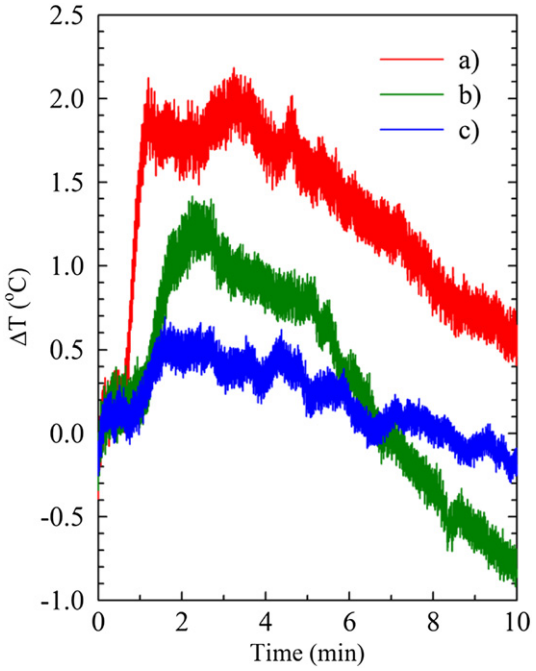

Fig. 9. The spatially-averaged ROI Δ*T* of anodes during electrochemical oxidation after exposure to wet ethanol (a) 700 °C, (b) 750 °C, and (c) 800 °C.

4. Discussion

Each of the techniques used in this study provides information pertinent to determining the viability of WE flows with H_2O:C_2H_5OH ratios of less than 3:1. The simplest metrics are the maximum current and power densities and resistances that are used to determine that the cells are functioning properly over the course of an experiment. The critical data are gathered by optical methods. The extent to which fuel flows are pyrolyzed or reformed prior to reaching the MEAs is determined with FTIR spectroscopy. NIR thermal imaging is used under a variety of conditions to determine, characterize and identify processes related to carbon formation as well as when and where on the anode they occur. Combining the *in situ* data gathered from all of the techniques with post-mortem analysis provides unique insight for the management of carbon-containing fuel feeds for use in SOFCs.

4.1. Electrochemical characterization

The focus of this work is the optical characterization of SOFC anode coking and degradation. Therefore, certain aspects of cell operation are not necessarily optimized for electrochemical performance. The direct result is that lower-than-expected current and power outputs are observed. While the factory characterization of cells in this study is considered proprietary information by MSRI, a few published studies are assumed to have used similar MEAs [12,53,54,58]. The current and power density maximums displayed in Fig. 1 are ∼10% of those reported elsewhere for similar cells. In the optical experiments, fuel and air flows are lower by a factor of 3–5 from those used by Zhao and Virkar in their characterization of similar cells [54]. Another unique optical design feature is the size of the current collector, which covers only ∼15% of the anode area to allow optical access to as much active surface as possible. The ability to electrochemically oxidize carbon deposits on the anode – as shown below and in previous work [17] – suggests that most of the anode is active. Therefore, densities are calculated using the area of the anode that is directly opposite the cathode, which is 2.40 cm^2. However, given the relatively small current collector (0.50 cm^2), electrochemical processes may not be as efficient in regions of the anode not under or directly adjacent to the current collector. If the current densities were calculated using the size of the current collector our values would increase by a factor of four and would be approximately half of the published values, even with gas flows that are not optimized.

Over the course of a given experiment, the total cell resistance decreases suggesting that operating the cells conditions the anode to expose more active area to the fuel stream. In contrast, the bulk

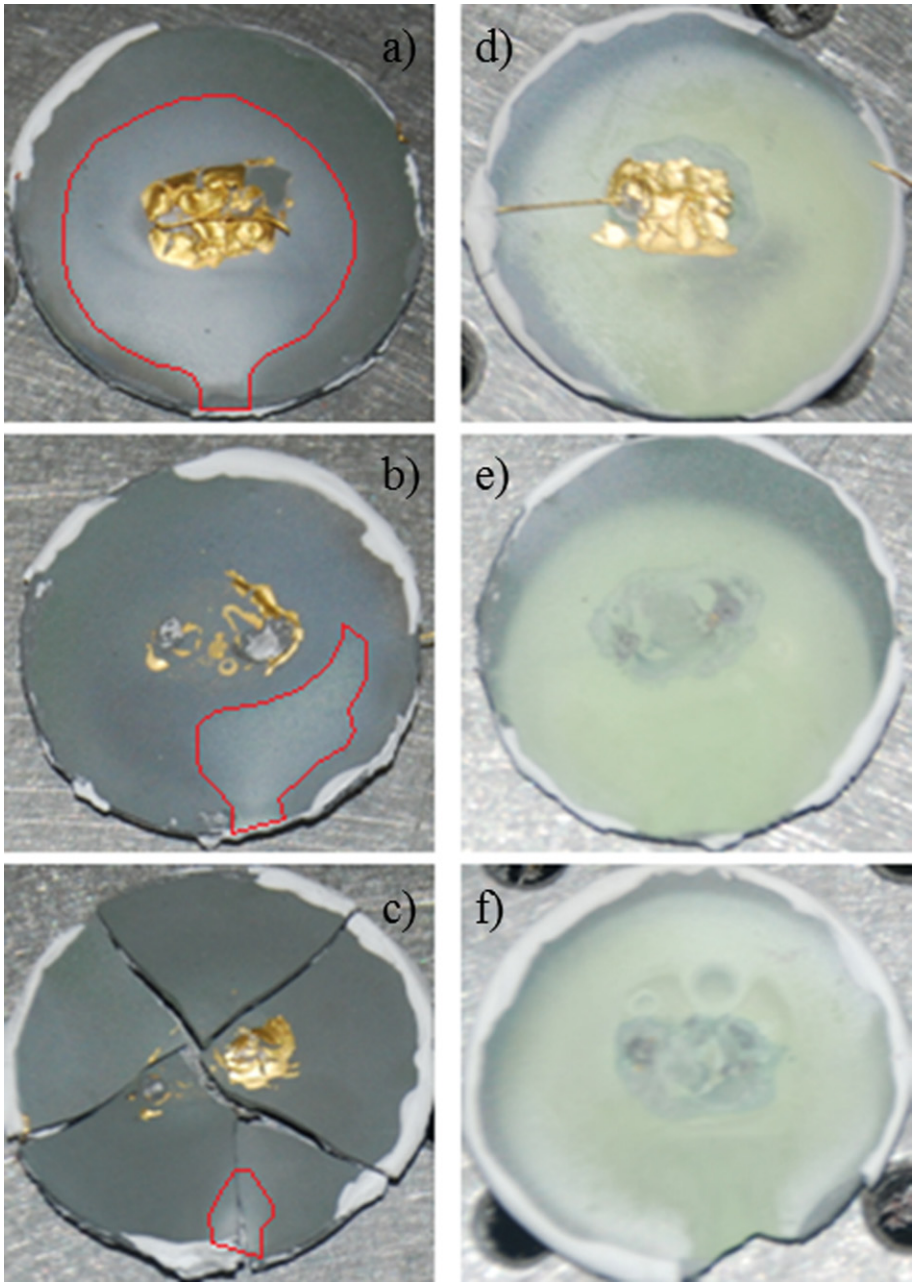

Fig. 10. Post-mortem photographs of cells after four-cycle experiments with (a) wet ethanol at 700 °C, (b) dry ethanol at 700 °C, (c) wet ethanol at 750 °C, (d) dry ethanol at 750 °C, (e) wet ethanol at 800 °C, (f) dry ethanol at 800 °C. Areas of discoloration/damage are outlined in red in (a), (b), and (c). (For interpretation of the references to color in this figure legend, the reader is referred to the web version of this article.)

resistance – generally associated with electrolyte loses – increases with each cycle. Therefore, the most likely cause of the drop in cell performance is strain in the thin YSZ layer due to the repeated expansion and contraction of the anode as it is cycled between oxidized, reduced, and carbon-poisoned states. Regardless, the small (5–10%) increase in the bulk resistance over the course of the experiment provides confidence in the accuracy of optical results regardless of when the data were gathered.

4.2. Gas-phase steam reforming of C_2H_5OH

Gas-phase FTIR spectral analysis of DE fuel flow found only minimal amounts of oxidized carbon in the form of CO at all three operational temperatures studied [17]. Species likely to form carbon deposits – C_2H_4 and C_6 species – become more prevalent as the temperature is increased, indicating that while pyrolysis progresses farther at higher temperatures, DE is not sufficiently reformed in this system to prevent carbon deposition under likely SOFC operating conditions.

The FTIR spectra of WE feeds are highly temperature dependent. The flow at 700 °C is still ~50% C_2H_5OH, while CH_4 and C_2H_4 combine to comprise ~20% of the flow. The fact that the flow is ~70% known-carbon forming species explains the relatively large amount of carbon observed on the surface by NIR imaging. Steam reforming simply does not oxidize enough of the carbon at 700 °C. As steam reforming becomes more efficient at higher temperatures, as determined by the increased abundance of CO in the WE feeds, it is reasonable to expect that non-oxidized carbon species would be consumed. However, gas-phase steam reforming alone is not enough to prevent anode coking. C_2H_4, the most abundant carbon-

deposit precursor observed, is 25% of the WE flow at 800 °C. The gas-phase composition is highly dependent on experimental parameters – *i.e.*, temperature profiles and residence time at elevated temperatures – making comparison to published studies difficult. The residence time of 0.4 s in this work means that the steam reforming process is not at the thermodynamic limit. Still, general commonalities exist with thermodynamic studies and experiments with longer residence times. Under equilibrium conditions with the same H_2O:C_2H_5OH ratio, CH_4 and C are more prevalent in underutilized fuel flows at 700 °C than at 800 °C [11]. This trend holds true in non-SOFC systems where fuel utilization is not a factor and H_2O:C_2H_5OH ratios are higher at 3:1 [59], with non-oxidized C species expected at all of the temperatures at which SOFCs are operated in this study. Given this, the presence of C_2H_4 and CH_4 in Fig. 4 is a reasonable result of incomplete steam reforming due to the short residence time.

The near-complete lack of damage on anodes at 800 °C suggests that there are processes at the anode that compensate for the incomplete gas-phase partial oxidation. Presumably, the oxidized species (CO, H_2O, and a small amount of CO_2) are abundant enough at higher temperatures to further reform the carbon-precursor products in the presence of the Ni/YSZ catalyst through a direct, internal reforming process. This presumption is supported by results published by Liberatori et al., [60] which demonstrate more complete conversion of C_2H_5OH at lower temperatures in the presence of a supported Ni catalyst. Therefore, the FTIR data lead one to infer that the reduction in carbon formation results from a combination of three factors: gas-phase steam reforming, internal reforming within the anode structure, and electrochemical fuel oxidation when the cells are polarized. The NIR imaging and gas-phase FTIR data combined explain not only the reduced amount of damage observed post-mortem, but also the voltage dependence of ΔT during WE exposure at 800 °C. Carbon formation no longer shields the camera from processes below the anode surface that counter the cooling of the anode when the cell is polarized – *i.e.*, fuel oxidation and resistive heating.

4.3. Carbon formation in SOFCs operated with WE

Experiments that mirror a previously published DE study [17] are used to determine if there are beneficial effects to using H_2O:C_2H_5OH ratios smaller than 3:1 in the WE flows. Anode surface cooling when DE was introduced as a fuel did not depend on ΔV_{OC}, indicating that endothermic fuel cracking and carbon deposition dominate anode chemistry. NIR images of the anodes of cells exposed to DE for 10 min (Fig. 11) show large spatial variations in anode surface temperature. These features correlate to regions of extreme MEA damage seen in post-mortem analysis. During WE experiments images and plotted, spatially-averaged ΔT's observed in the ROI show a strong temperature dependence on the interactions of the WE stream with the anode. The images in Fig. 5 show more intense cooling at lower temperatures, which is a potential indication that anodes are more susceptible to carbon formation during exposure to WE at temperatures below 800 °C. Furthermore, ΔT's do not exhibit the voltage dependence (Fig. 7) at lower temperatures that are observed at 800 °C. This indicates that carbon deposits to an extent that partially shields the camera from heating processes, as in the DE cases. An interesting aspect of the ΔT data is that at all of the voltages studied, cells at 750 °C cool the most. This phenomenon is also observed for cells operated with DE. Speculatively, this is attributed to the inverse behavior of the two processes most likely to be responsible for surface cooling during fuel exposure. Cracking of fuel molecules on the Ni catalyst proceeds faster at higher temperatures, resulting in more cooling from the endothermic process at 800 °C. The other process that results in the observation of lower surface temperatures is the formation of carbon, which causes the surface to appear cooler by ~2 °C due to a change in emissivity [17,50]. In light of the gas-phase FTIR results, cells at lower operational temperatures are more susceptible to coking. While both processes are likely to occur at all three of the operational temperatures, there appears to be a synergistic effect at 750 °C that results in more intense cooling at that temperature.

It should be noted that the error bars in Fig. 7 correspond to cell-to-cell variations. While attempts were made to achieve consistency in our experiments, each time the SOFC manifold is assembled the shape of the spatial variations in temperature change slightly due to small differences between cells and changes in the fuel flow trajectory. Therefore, while the ROI is always horizontally centered in the area between the fuel inlet and the current collector, the fuel flow path is not perfectly aligned to the central *y*-axis of the cell in each experiment and is not necessarily symmetric. If the fuel flow path is shifted slightly off center, less of the ROI will encompass the area that experiences the most intense ΔT. Given that the changes in the stream are typically subtle, changing the ROI to account for the arbitrary shapes of the flow path could result in more inconsistencies in the results. Under conditions that result in a small amount of spatial variation (800 °C) the effect of a change in the flow path is minimized, leading to less cell-to-cell variation. Cells operated at 750 and 700 °C display large overall spatial variation, the shifting of which in each individual assembly leads to the relatively large error bars.

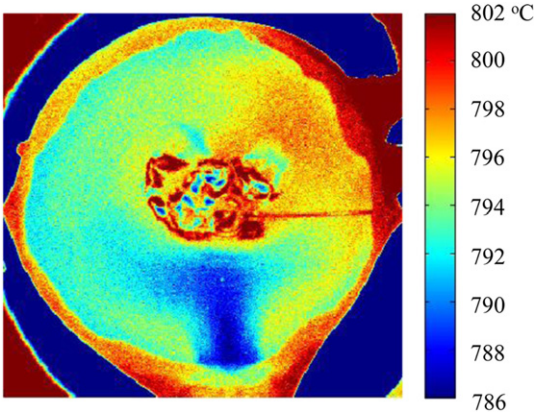

Fig. 11. False-color thermal image of a SOFC anode after 10 min of exposure to dry ethanol at OCV and a nominal operational temperature of 800 °C.

4.4. Determination of relative amounts of carbon formation by electrochemical oxidation

Exposure of Ni/YSZ anodes to fuel flows with H_2O:C_2H_5OH ratios suggested by Cimenti and Hill [11] leads to diminished surface cooling. NIR imaging data collected during WE exposure indicate carbon formation at 700 and 750 °C. The maximum ΔT in cells operated with WE at 800 °C is ~2 °C (Figs. 7 and 8), which is less than any of the carbon-containing fuels studied by this method, including CH_3OH, which was shown to form negligible amounts of carbon at 800 °C [17,49]. However, it is difficult to determine if carbon formation on anode surfaces has been completely suppressed from the thermal data gathered during fuel exposure. Productive endothermic processes, such as fuel cracking, may mask the deposition of small amounts of carbon.

The relative amounts of carbon formed on the Ni anode catalyst can be qualitatively determined by electrochemically oxidizing the anode. Previous work has shown that anodes not exposed to carbon initially heat as the Ni anode is oxidized [50]. Within 6 min the

surface temperature drops below the temperature of the surface prior to oxidation, indicating that the anode oxidation has completed. Anodes exposed to carbon-forming fuels have temporal oxidation profiles that show prolonged heating, resulting in ΔT's that remain above 0 °C for the duration of a 10 min experiment. The time needed for the oxidative heating profile to return to 0 °C is a useful metric for determining the presence of carbon on the anodes. Anodes exposed to CH_3OH at 800 °C exhibited voltage-dependent cooling while fuel was flowing; however, the oxidation time profile displayed sustained increases in temperature [17]. This indicates that carbon was formed, but in small enough amounts that it could not be detected during fuel exposure.

The heating due to electrochemical oxidation of anodes after exposure to WE flow (Fig. 9) corresponds well to the conclusions drawn from thermal data acquired while fuels are flowing. Cells operated at 700 °C exhibit the most intense heating and ΔT remains above 0 °C for the entire 10 min. This behavior suggests that steam reforming does not partially oxidize enough C_2H_5OH to prevent anode coking. The oxidative heating profile of the cell at 800 °C shows a small amount of initial heating, but ΔT reaches 0 °C at 6 min, eventually dropping below. This behavior is similar to cells that have not been exposed to carbon. Considered with the voltage-dependent behavior of cells exposed to WE at 800 °C, this result provides evidence that negligible carbon forms at 800 °C over the course of a 10 min exposure. Cells operated at 750 °C also have heating profiles similar to cells operated without carbon-containing fuels. As in the 800 °C case, ΔT drops below 0 °C at approximately 6 min. While this is encouraging, the spatial variations in ΔT and the lack of voltage dependence observed under fuel flows is concerning. The apparent disagreement between the data collected during WE flow and during electrochemical oxidation is evidence that 750 °C is the temperature below which the WE flows with reduced H_2O content lead to anode coking, but above which these flows become viable.

4.5. Ultimate cell conditions from ex situ photos

The photographs in Fig. 10 correlate well with the *in situ* data. The false-color NIR images and horizontal profiles of the anodes under fuel flows display spatial temperature variations that correlate with evidence of carbon-related anode deterioration, and could be monitored in real time. Notably, cells run at 800 °C show such a small amount of damage, in both *in situ* and *ex situ* results, that discoloration is determined to be a product of operation at OCV. This is confirmed by a total lack of anode discoloration on MEAs in separate experiments that follow the same protocol with the exception that cells are always exposed to WE while at 0.6 V ΔV_{OC}, never at OCV (see Supporting information). Steam reforming with a 1.12 H_2O:C_2H_5OH ratio is considered to be sufficient for clean C_2H_5OH use when cells are polarized. This result is in agreement with previous results indicating that steam reforming generally does not occur extensively or rapidly at temperatures below 800 °C [34]. Thermal data indicate that steam reforming of C_2H_5OH at 800 °C with reduced H_2O content proceeds at a rapid enough pace to prevent damage to the Ni/YSZ cermet – even at the 0.4 s residence time. It is also clear that operating at H_2O:C_2H_5OH ratios <3:1 does not totally prevent carbon damage at all operational temperatures.

5. Conclusions

The benefits of direct steam reforming of C_2H_5OH fuel in SOFCs have been demonstrated optically for the first time using NIR thermal imaging of Ni/YSZ anode surfaces. Thermal data are correlated to post-mortem photographs of the MEAs and gas-phase FTIR spectroscopic assessments of fuel flow compositions. It is determined that fuel flows that are humidified to H_2O:C_2H_5OH ratios of 1.58, 1.27, and 1.12 at 700, 750, and 800 °C, respectively, result in far less damage to the anode than DE fuel. However, damage is not completely avoided at 700 or 750 °C as determined by subtle spatial variations in anode surface temperatures that appear clearly in the NIR images. Steam participates in fuel reforming in the gas phase as shown by the much lower concentrations of C_2H_5OH and significant concentrations of CO in the FTIR spectra of the WE feed reaching the anode. However, CH_4 and C_2H_4 – an olefin and known carbon-deposit precursor – are still present. As such, it is determined that internal steam reforming occurs both in the gas phase and at the anode catalyst, partially oxidizing more C_2H_5OH and deposit precursors than the pyrolysis of DE. Thermal imaging and post-mortem analysis confirm that the WE flows at 800 °C form negligible amounts of carbon deposits in polarized cells, resulting in minimal MEA deterioration.

These results are specific to a unique button cell SOFC system, but they serve as benchmark data for the further development of direct, internal reforming SOFC systems, especially in smaller, portable systems. The success in limiting or removing the deleterious effects of C_2H_5OH fuel at 800 °C – specifically when cells are polarized – is a promising result with regards to the logistical issues related to water supply for SOFCs as the H_2O:C_2H_5OH ratio used in this work is well below the >3:1 ratios suggested elsewhere. The small surface temperature variations detected *in situ* by our NIR camera provide real-time analysis of the early stages of SOFC failure, demonstrating the promise of this convenient imaging technique for system diagnostics capable of aiding SOFC development and operational protocol in a variety of systems.

Acknowledgments

Support for this work was provided by the Office of Naval Research. The authors acknowledge David A. Kidwell at NRL for help with early development of this project, Bryan W. Eichhorn at the University of Maryland College Park, Anthony M. Dean at the Colorado School of Mines, and Robert A. Walker at Montana State University for helpful discussions.

Appendix A. Supplementary data

Supplementary data related to this article can be found at http://dx.doi.org/10.1016/j.jpowsour.2013.01.048.

References

[1] R.M. Ormerod, Chem. Soc. Rev. 32 (2003) 17–28.
[2] H. Qin, Z. Zhu, Q. Liu, Y. Jing, R. Raza, S. Imran, M. Sing, G. Abbas, B. Zhu, Energ. Environ. Sci. 4 (2011) 1273–1276.
[3] S.L. Douvartzides, F.A. Coutelieris, A.K. Demin, P.E. Tsiakaras, AIChE J. 49 (2003) 248–257.
[4] D.J.L. Brett, A. Atkinson, N.P. Brandon, S.J. Skinner, Chem. Soc. Rev. 37 (2008) 1568–1578.
[5] F.Z. Chen, S.W. Zha, J. Dong, M.L. Liu, Solid State Ionics 166 (2004) 269–273.
[6] A.L. Dicks, J. Power Sources 71 (1998) 111–122.
[7] R.J. Kee, H. Zhu, A.M. Sukeshini, G.S. Jackson, Combust. Sci. Technol. 180 (2007) 1207–1244.
[8] N. Laosiripojana, S. Assabumrungrat, J. Power Sources 163 (2007) 943–951.
[9] S. Bebelis, S. Neophytides, Solid State Ionics 152-153 (2002) 447–453.
[10] M. Cimenti, V. Alzate-Restrepo, J.M. Hill, J. Power Sources 195 (2010) 4002–4012.
[11] M. Cimenti, J.M. Hill, J. Power Sources 186 (2009) 377–384.
[12] Y. Jiang, A.V. Virkar, J. Electrochem. Soc. 148 (2001) A706–A709.
[13] M.F. Liu, R.R. Peng, D.H. Dong, J.F. Gao, X.Q. Liu, G.Y. Meng, J. Power Sources 185 (2008) 188–192.
[14] L. Mingfei, P. Ranran, D. Dehua, G. Jianfeng, L. Xingqin, M. Guangyao, J. Power Sources (2008) 188–192.
[15] M. Mogensen, K. Kammer, Annu. Rev. Mater. Res. 33 (2003) 321–331.
[16] M.B. Pomfret, J. Marda, G.S. Jackson, B.W. Eichhorn, A.M. Dean, R.A. Walker, J. Phys. Chem. C 112 (2008) 5232–5240.

[17] M.B. Pomfret, D.A. Steinhurst, J.C. Owrutsky, Energy Fuels 25 (2011) 2633–2642.
[18] K.L. Randolph, A.M. Dean, Phys. Chem. Chem. Phys. 9 (2007) 4245–4258.
[19] K. Sasaki, H. Kojo, Y. Hori, R. Kikuchi, K. Eguchi, Electrochemistry 70 (2002) 18–22.
[20] P. Tsiakaras, A. Demin, J. Power Sources 102 (2001) 210–217.
[21] S.A. Venancio, T.F. Gutierres, B.J.M. Sarruf, P.E.V. Miranda, Materia-Rio De Janeiro 13 (2008) 560–568.
[22] A. Aguadero, C. de la Calle, J.A. Alonso, D. Perez-Coll, M.J. Escudero, L. Daza, J. Power Sources 192 (2009) 78–83.
[23] M. Cimenti, J.M. Hill, J. Power Sources 195 (2010) 3996–4001.
[24] B. Huang, S.R. Wang, R.Z. Liu, T.L. Wen, J. Power Sources 167 (2007) 288–294.
[25] B. Huang, S.R. Wang, R.Z. Liu, X.E. Ye, H.W. Nie, X.E. Sun, T.L. Wen, J. Power Sources 167 (2007) 39–46.
[26] S.P. Jiang, Y.M. Ye, T.M. He, S.B. Ho, J. Power Sources 185 (2008) 179–182.
[27] S. McIntosh, H. He, S.-I. Lee, O. Costa-Nunes, V. Krishnan, J.M. Vohs, R.J. Gorte, J. Electrochem. Soc. 151 (2004) A604–A608.
[28] X.F. Ye, B. Huang, S.R. Wang, Z.R. Wang, L. Xiong, T.L. Wen, J. Power Sources 164 (2007) 203–209.
[29] X.F. Ye, S.R. Wang, Q. Hu, J.Y. Chen, T.L. Wen, Z.Y. Wen, Solid State Ionics 180 (2009) 276–281.
[30] X.F. Ye, S.R. Wang, Z.R. Wang, Q. Hu, X.F. Sun, T.L. Wen, Z.Y. Wen, J. Power Sources 183 (2008) 512–517.
[31] D. Srinivas, C.V.V. Satyanarayana, H.S. Potdar, P. Ratnasamy, Appl. Catal. A Gen. 246 (2003) 323–334.
[32] K. Sasaki, K. Watanabe, Y. Teraoka, J. Electrochem. Soc. 151 (2004) A965–A970.
[33] L.E. Arteaga, L.M. Peralta, V. Kafarov, Y. Casas, E. Gonzales, Chem. Engin. J. 136 (2008) 256–266.
[34] S. Diethelm, J. Van herle, J. Power Sources 196 (2011) 7355–7362.
[35] J.M. Klein, M. Henault, C. Roux, Y. Bultel, S. Georges, J. Power Sources (2009) 331–337.
[36] M. Cimenti, J.M. Hill, J. Power Sources 195 (2010) 54–61.
[37] T.S. Norton, F.L. Dryer, Int. J. Chem. Kinet. 22 (1990) 219–241.
[38] B.C. Eigenbrodt, M.B. Pomfret, D.A. Steinhurst, J.C. Owrutsky, R.A. Walker, J. Phys. Chem. C 115 (2011) 2895–2903.
[39] S. Assabumrungrat, N. Laosiripojana, V. Pavarajarn, W. Sangtongkitcharoen, A. Tangjitmatee, P. Praserthdam, J. Power Sources 139 (2005) 55–60.
[40] P. Dokamaingam, S. Assabumrungrat, A. Soottitantawat, N. Laosiripojana, Int. J. Hydrogen Energy 34 (2009) 6415–6424.
[41] G.K. Gupta, A.M. Dean, K. Ahn, R.J. Gorte, J. Power Sources 158 (2006) 497–503.
[42] A. Arpornwichanop, N. Chalermpanchai, Y. Patcharavorachot, S. Assabumrungrat, M. Tade, Int. J. Hydrogen Energy 34 (2009) 7780–7788.
[43] G. Vourliotakis, G. Skevis, M.A. Founti, Int. J. Hydrogen Energy 34 (2009) 7626–7637.
[44] T.S. Lee, J.N. Chung, Y.C. Chen, Energy Convers. Manag. 52 (2011) 3214–3226.
[45] M.B. Pomfret, J.C. Owrutsky, R.A. Walker, Annu. Rev. Anal. Chem. 3 (2010) 151–174.
[46] M.B. Pomfret, R.A. Walker, J.C. Owrutsky, J. Phys. Chem. Lett. 3 (2012) 3053–3064.
[47] X. Lu, P.W. Faguy, M. Liu, J. Electrochem. Soc. 149 (2002). A1293–A129`8.
[48] M.B. Pomfret, J.C. Owrutsky, R.A. Walker, Anal. Chem. 79 (2007) 2367–2372.
[49] M.B. Pomfret, D.A. Steinhurst, D.A. Kidwell, J.C. Owrutsky, Electrochem. Soc. Trans. 25 (2009) 839.
[50] M.B. Pomfret, D.A. Steinhurst, D.A. Kidwell, J.C. Owrutsky, J. Power Sources 195 (2010) 257–262.
[51] D.J.L. Brett, P. Aguiar, R. Clague, A.J. Marquis, S. Schottl, R. Simpson, N.P. Brandon, J. Power Sources 166 (2007) 112–119.
[52] G. Ju, K. Reifsnider, X.Y. Huang, J. Fuel Cell Sci. Technol. 5 (2008) 6.
[53] N.M. Tikekar, T.J. Armstrong, A.V. Virkar, J. Electrochem. Soc. 153 (2006) A654–A663.
[54] F. Zhao, A.V. Virkar, J. Power Sources 141 (2005) 79–95.
[55] C. Esarte, A. Callejas, A. Millera, R. Bilbao, M.U. Alzueta, Fuel 90 (2011) 844–849.
[56] C. Esarte, A. Millera, R. Bilbao, M.U. Alzueta, Fuel Process. Technol. 90 (2009) 496–503.
[57] A. Singh, J.M. Hill, J. Power Sources 214 (2012) 185–194.
[58] C.C. Xu, M.Y. Gong, J.W. Zondlo, X.B. Liu, H.O. Finklea, J. Power Sources 195 (2010) 2149–2158.
[59] C.N. de Avila, C.E. Hori, A.J. de Assis, Energy 36 (2011) 4385–4395.
[60] J.W.C. Liberatori, R.U. Ribeiro, D. Zanchet, F.B. Noronha, J.M.C. Bueno, Appl. Catal. A Gen. 327 (2007) 197–204.